The Astrophysical Journal, 591:446–453, 2003 July 1

HELIOSEISMIC OBSERVATION OF THE STRUCTURE AND DYNAMICS OF A ROTATING SUNSPOT BENEATH THE SOLAR SURFACE

Junwei Zhao and Alexander G. Kosovichev
W. W. Hansen Experimental Physics Laboratory, Stanford University, Stanford, CA 94305-4085; junwei@quake.stanford.edu
Received 2003 January 22; accepted 2003 March 13

ABSTRACT

Time-distance helioseismology is applied to study the subphotospheric structures and dynamics of an unusually fast-rotating sunspot observed by the Michelson Doppler Imager on board *SOHO* in 2000 August. The subsurface sound speed structures and velocity fields are obtained for the sunspot region at different depths from 0 to 12 Mm. By comparing the subsurface sound speed variations with the surface magnetic field, we find evidence for structural twists beneath the visible surface of this active region, which may indicate that magnetic twists often seen at the photosphere also exist beneath the photosphere. We also report on the observation of subsurface horizontal vortical flows that extend to a depth of 5 Mm around this rotating sunspot and present evidence that opposite vortical flows may exist below 9 Mm. It is suggested that the vortical flows around this active region may build up a significant amount of magnetic helicity and energy to power solar eruptions. Monte Carlo simulation has been performed to estimate the error propagation, and in addition the sunspot umbra is masked to test the reliability of our inversion results. On the basis of the three-dimensional velocity fields obtained from the time-distance helioseismology inversions, we estimate the subsurface kinetic helicity at different depths for the first time and conclude that it is comparable to the current helicity estimated from vector magnetograms.

Subject headings: Sun: helioseismology — Sun: interior — Sun: oscillations — sunspots

1. INTRODUCTION

Sunspots that exhibit some degrees of rotational motions around their own vertical axes are not rare in solar observations (Knoška 1975). Many authors (e.g., Tokman & Bellan 2002) suggested that some solar eruptive events, such as solar flares and coronal mass ejections, are correlated with rotational and sheared motions of sunspots. Recently, Brown et al. (2003) studied several rotating sunspots observed by *TRACE* and calculated the total magnetic helicity and energy generated by the sunspot rotation. They found that the sunspot rotation can twist coronal loops and trigger solar flares. On the other hand, many authors investigated the origin of the magnetic twists observed in vector magnetograms and coronal loop structures, and some explanations have been proposed, including the solar differential rotation, surface motions, and turbulent motions in the solar convection zone (see reviews by Canfield & Pevtsov 2000). More recently, based on analysis of 22 bipolar solar active regions, López Fuentes et al. (2003) proposed that the magnetic deformation may result from large-scale vortical flows in the solar convection zone and the photosphere or in subphotospheric layers. Therefore, it is of great importance and interest to investigate the subsurface structures and dynamics of rotating sunspots. These studies may shed light on physical conditions in the solar convection zone, the interaction between convective motions and magnetic structures of sunspots, the formation of magnetic twists, the energy storage for solar eruptions, and many other interesting topics of solar physics.

Recently, several local helioseismology methods have been developed to derive the interior sound speed structures and flow fields for sunspots (e.g., Duvall et al. 1993; Lindsey & Braun 2000; Braun & Lindsey 2000; Chou 2000; Haber et al. 2000). Time-distance helioseismology (Duvall et al. 1993, 1996) is one of the local helioseismology techniques used to infer both large-scale and small-scale structures and flow fields inside the Sun. For large scales, Giles (1999) derived meridional flows and zonal flows and obtained results that were in reasonable agreement with those from the global helioseismology technique of frequency splitting of normal modes. For small scales, Kosovichev, Duvall, & Scherrer (2000) and Zhao, Kosovichev, & Duvall (2001) obtained the sound speed structures and flow fields more than 10 Mm deep beneath a sunspot. At the same time, the forward problems (Gizon & Birch 2002) and numerical modeling (Birch & Kosovichev 2000; Jensen, Jacobsen, & Christensen-Dalsgaard 2000) for the time-distance helioseismology have also been addressed. Based on Fresnel zone sensitivity kernels, Jensen et al. (2001) inferred the sound speed perturbation structures beneath a developing active region and found similar results obtained from the ray approximation results (Kosovichev et al. 2000). This indicates that inversion of sunspot structures and flow fields based on the ray approximation gives reasonably good results on scales comparable to the acoustic wavelength. This is also demonstrated by numerical tests of Birch et al. (2001), which showed that small-scale features can be resolved only by using a complete wave theory for data inversion and that the inversion methods based on the ray approximation may underestimate the magnitude of small-scale perturbations. However, at the larger scales comparable to the first Fresnel zone, the ray approximation works well. But given complicated averaging and regularization in the data inversion procedure and the great number of data points involved in the inversion, it is not yet clear how the ray approximation will eventually affect the inversion results. The ray approximation is still used in this work

because no computationally efficient wave inversion has yet been developed, and it is safe to assume that this approximation provides qualitatively correct results.

In this paper, we apply the method of time-distance helioseismology to a fast-rotating sunspot observed by the Michelson Doppler Imager (MDI) on board *SOHO* in 2000 August and present maps of subsurface flows and sound speed variations that provide evidence for subsurface horizontal vortices and structural twists in the interior of this sunspot region. The observations and the inversion procedure are described in § 2, and the inversion results from *SOHO*/MDI data are presented in § 3. Error analysis is given in § 4, followed by discussion in § 5.

2. OBSERVATIONS AND INVERSIONS

2.1. *SOHO*/*MDI Observations*

The full-disk Dopplergrams with 1 minute cadence used for our analyses were obtained from the Michelson Doppler Imager (MDI) aboard *SOHO* (Scherrer et al. 1995). The spatial resolution is 2″, corresponding to 0.119 heliographic degrees per CCD pixel (1 heliographic degree [1°] corresponds approximately to 12.15 Mm on the solar surface).

Active region NOAA 9114 passed through the solar disk from 2000 August 4 to August 12. The movie made from the MDI magnetograms with a temporal interval of 96 minutes from August 6 to August 10 showed in this active region a fast-rotating leading large sunspot and a small satellite sunspot moving closer to the leading sunspot and merging with it on August 8. After the merge, the sunspot continued its rotation until August 10. The sunspot's rotation is clearly seen because the larger sunspot is not completely round but has a protruding feature, marked "A" in Figure 1. It shows counterclockwise rotation around the main sunspot. Although rotation of sunspots is not rare in solar observations, such a rapid and large degree of rotation (approximately 200° within 3 days) is rather unusual.

Figure 1 shows a magnetogram obtained by *SOHO*/MDI at 1611 UT on August 7. The trace of the small sunspot from 0000 UT on August 6 to 0800 UT on August 10 is plotted as a solid line in Figure 1, with asterisks marking 0000 UT of every day from August 6 to 10. The small sunspot moved along a curve rather than a straight line before the merge, and after merging with the larger sunspot it rotated together with this sunspot.

To perform the time-distance helioseismology measurements with an acceptable signal-to-noise ratio, we need at least 512 uninterrupted 1 minute cadence Dopplergrams. The following two observing periods, which meet this requirement, were selected for our time-distance analyses: 1620 UT August 7–0051 UT 2000 August 8 and 0408 UT–1239 UT 2000 August 8 (for simplicity, we refer to these as the August 7 data and the August 8 data, respectively).

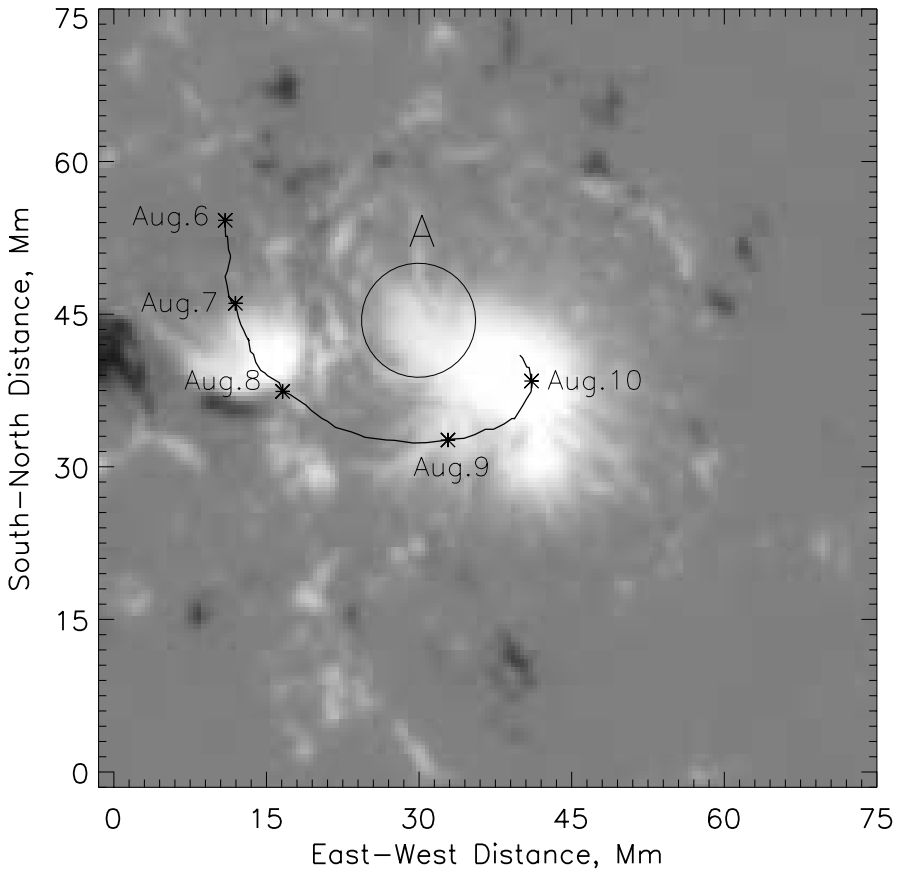

FIG. 1.—Line-of-sight magnetogram obtained by *SOHO*/MDI at 1611 UT on 2000 August 7. The solid line shows the trace of the small sunspot from 0000 UT August 6 to 0800 UT August 10. Asterisks mark 0000 UT August 6 through August 10, respectively. The protruding part from the larger sunspot in the circle is marked as feature A. The magnetic field strength ranges from −1100 to 1600 G.

2.2. *Time-Distance Measurement and Inversion*

The method of time-distance helioseismology was originally proposed by Duvall et al. (1993, 1996). Giles (1999) has thoroughly discussed the measurement procedures for *SOHO*/MDI data, including remapping, data filtering, model fitting, and error estimation. Following the procedure described in Giles (1999), we have measured the travel time differences for acoustic waves propagating in opposite directions along different ray paths in the selected solar area. Inversion of these propagation time differences provides us with maps of sound speed variations and flow fields beneath the visible surface at different depths.

The inverse problem of time-distance helioseismology was first addressed by Kosovichev (1996) on the basis of the ray approximation. Later it was used by Giles (1999) to derive the solar large-scale flows and by Zhao et al. (2001) to derive the small-scale flow fields beneath a sunspot. Kosovichev (1996) and Zhao et al. (2001) carried out the inversions by employing the algorithm LSQR (Paige & Saunders 1982), a well-tested and widely used algorithm in the inverse problems of Earth's seismology. They tested the accuracy and convergence of the LSQR algorithm using artificial data and found that this technique can recover three-dimensional flow structures up to about 15 Mm beneath the visible surface. A more detailed description and discussion of the application of LSQR to helioseismology inversions can be found in Kosovichev (1999). This algorithm represents an iterative conjugate-gradient method of solving least-squares problems for large sparse systems of linear equations. It is based on the Lanczos bidiagonalization and is very efficient, typically requiring a few iterations for our problems. Recently, Zhao & Kosovichev (2003) employed another inversion technique, multichannel deconvolution (MCD), proposed by Jacobsen et al. (1999) to derive the flow fields beneath a sunspot, and compared the results from the LSQR algorithm. The results from these two different inversion techniques were in good agreement, with correlation coefficients above 95% for the three-dimensional velocities at the corresponding depths. The results presented in this paper are calculated by the LSQR algorithm, although the MCD technique was also employed to ascertain results.

Here we present some additional inversion tests for noise-free artificial data to estimate the ability of the LSQR-based inversion technique to measure vortical flows and detect opposite flows within relatively short depth ranges. Figure 2 (*top*) shows the original artificial data, with downward and converging counterclockwise vortical flows at the depth of 0–3 Mm, and upward and diverging clockwise flows at the depth of 9–12 Mm. Figure 2 (*bottom*) shows the inversion results from the artificial data following the procedure of

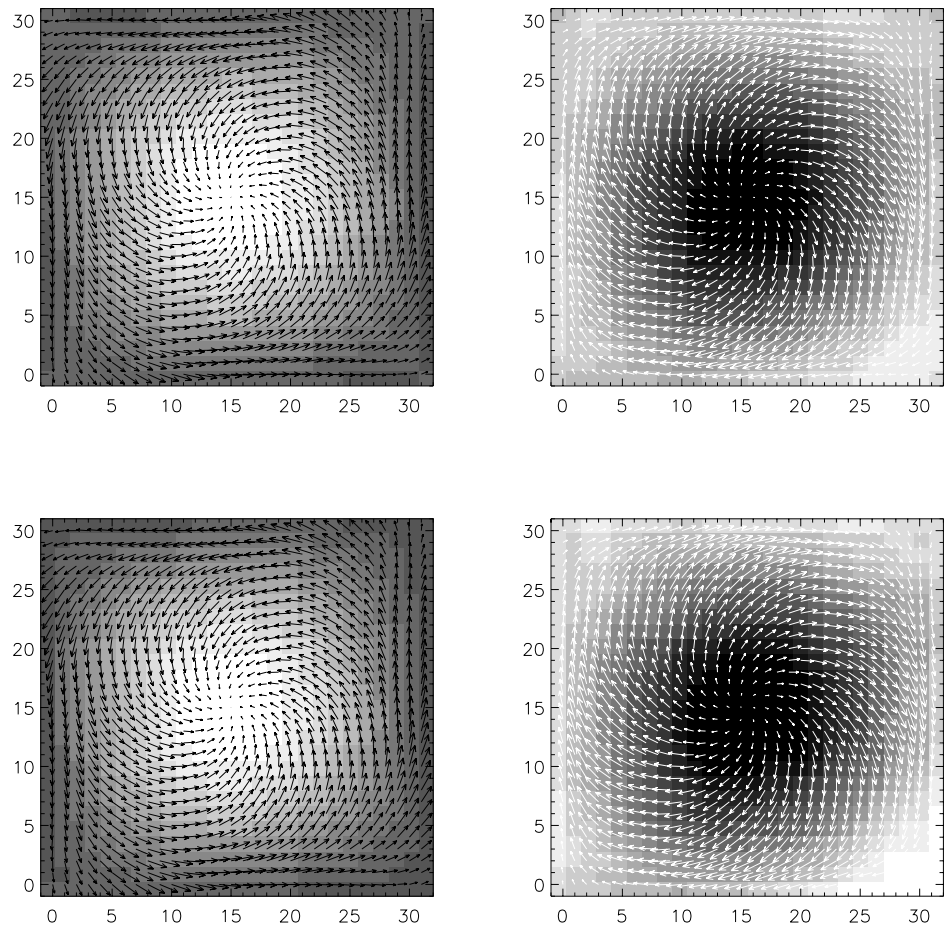

FIG. 2.—Test results from noise-free artificial data. Background images in each graph represent the vertical velocities, showing upward (*bright*), downward (*gray*), and horizontal flows (*arrows*). *Top*, Artificial data for the depth of 0–3 Mm (*left*) and 9–12 Mm (*right*); *bottom*, inversion results. Scales are arbitrary in these graphs.

Zhao et al. (2001). We find that the inversion results reproduce very well the flow patterns of the artificial data, with the correlation coefficient as high as 98.9% for the depth of 0–3 Mm and 94.7% for 9–12 Mm.

3. RESULTS

3.1. *Results of Sound Speed Variation*

Previous observations have shown that the average sound speed variation $\delta c/c$ relative to the quiet Sun is mostly positive below the depth of ~4 Mm in active regions (Kosovichev et al. 2000; Sun et al. 2002). We may assume that the horizontal shape of the subsurface sound speed variation corresponds to the shape of the subsurface magnetic field structure; however, the precise relation between them has not been established.

In Figure 3 (*left*), the background image shows the sound speed variation structure at the depth of 6 Mm, obtained from the August 7 data. The contour lines in this graph show the line-of-sight magnetic field averaged from all 1 minute cadence magnetograms during the 512 minute observation period. Even though the exact correspondence between the photospheric structures and the subsurface sound speed structures cannot be easily seen, it appears that the subsurface structure is rotated by ~34° counterclockwise with respect to the photospheric sunspot structure. The root of the small sunspot that eventually merged with the larger sunspot is not identified as a separate structure in our data. This may imply that the root of the small satellite sunspot was probably connected to the magnetic flux clusters of the main sunspot deeper than the depth of a few megameters (see also Kosovichev et al. 2000).

Figure 3 (*right*) shows the sound speed variation map and the averaged line-of-sight magnetic field from the August 8 data. In this case, the shape of the sound speed variation is not in the same good accordance with the shape of the surface magnetic field as in Figure 3 (*left*). However, the protruding part of the sound speed structure seems to correspond well to feature A on the surface, thus forming an angle of ~45° between these features. These observations seem to suggest the existence of the subsurface structural twist of the sunspot in both data sets.

3.2. *Flow Fields Beneath the Surface*

Three-dimensional velocity maps have also been obtained from the August 7 and 8 data. Figure 4 (*left*) present the velocity fields at two depth intervals, 0–3 and 9–12 Mm, obtained from the August 7 data, while Figure 4 (*right*) shows the velocity fields at the same depth intervals for the August 8 data.

In the upper layer (0–3 Mm in depth), we find strong converging flows with downdrafts in the sunspot area, as found by Zhao et al. (2001). Except for the lower left corner (or the southeast part) of the main sunspot, an apparent counterclockwise vortical flow can be found around the sunspot for both August 7 and 8, with stronger vorticity on August 8. This vortex has the same counterclockwise direction as the sunspot surface rotation. Similar vortical flow patterns are found at the depth of 3–5 Mm, which implies that the rotational motions seen at the surface extends to 5 Mm in depth.

In the deeper layer (9–12 Mm in depth), we observe that divergent flows with upward flows replace the converging downflows in the sunspot area. A strong clockwise vortex can be seen in the August 8 graph (Fig. 4*d*) in and around the sunspot region. The August 7 data (Fig. 4*b*) also show this vortex but it has a smaller vorticity. It appears that the direction of the vortex seen at this depth is opposite to the surface rotation of the sunspots.

To show more clearly the vortical flows in and around the sunspot region, we present in Figure 5 the tangential components of the velocities relative to the center of the sunspot at two different depths from the August 8 data.

3.3. *Kinetic Helicity*

The three-dimensional velocity field obtained from our time-distance helioseismological inversions enables us to estimate the kinetic helicity of the subsurface flows, which is an important characteristic quantity for solar MHD. We define the kinetic helicity as $\alpha^v \equiv \boldsymbol{v} \cdot (\nabla \times \boldsymbol{v})/|\boldsymbol{v}|^2$

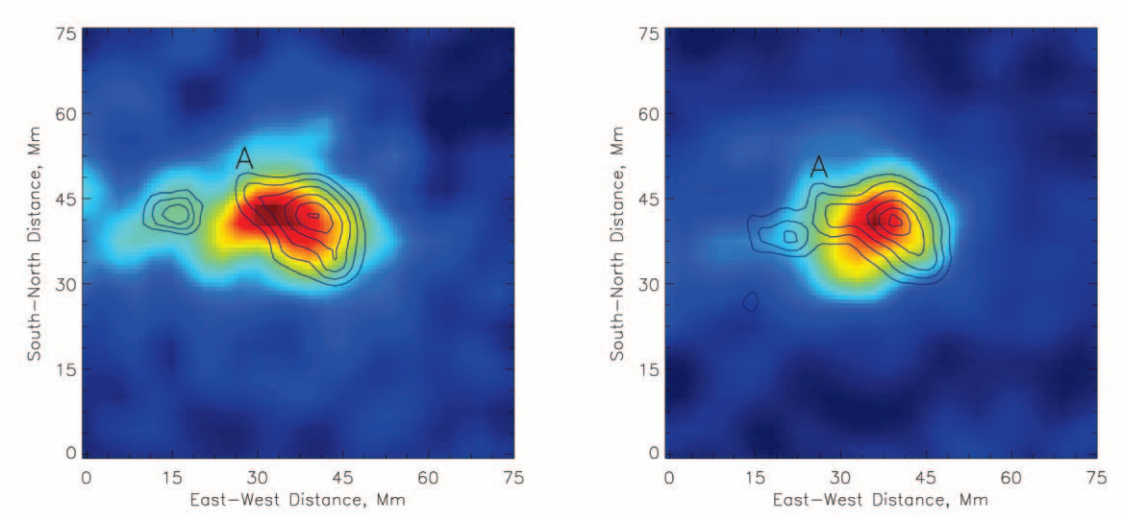

FIG. 3.—Sound speed variation maps at the depth of 6 Mm (*background color images*) and the photospheric line-of-sight magnetic field (*contour lines*) for two observing intervals: *left*, 1620 UT 2000 August 7–0051 UT 2000 August 8; *right*, 0408 UT August 8–1239 UT 2000 August 8. Red corresponds to positive sound speed variation $\delta c/c$, and blue to negative $\delta c/c$, which ranges from −0.02 to 0.08. The contour levels are 600, 800, 1000, 1200, 1400, and 1600 G.

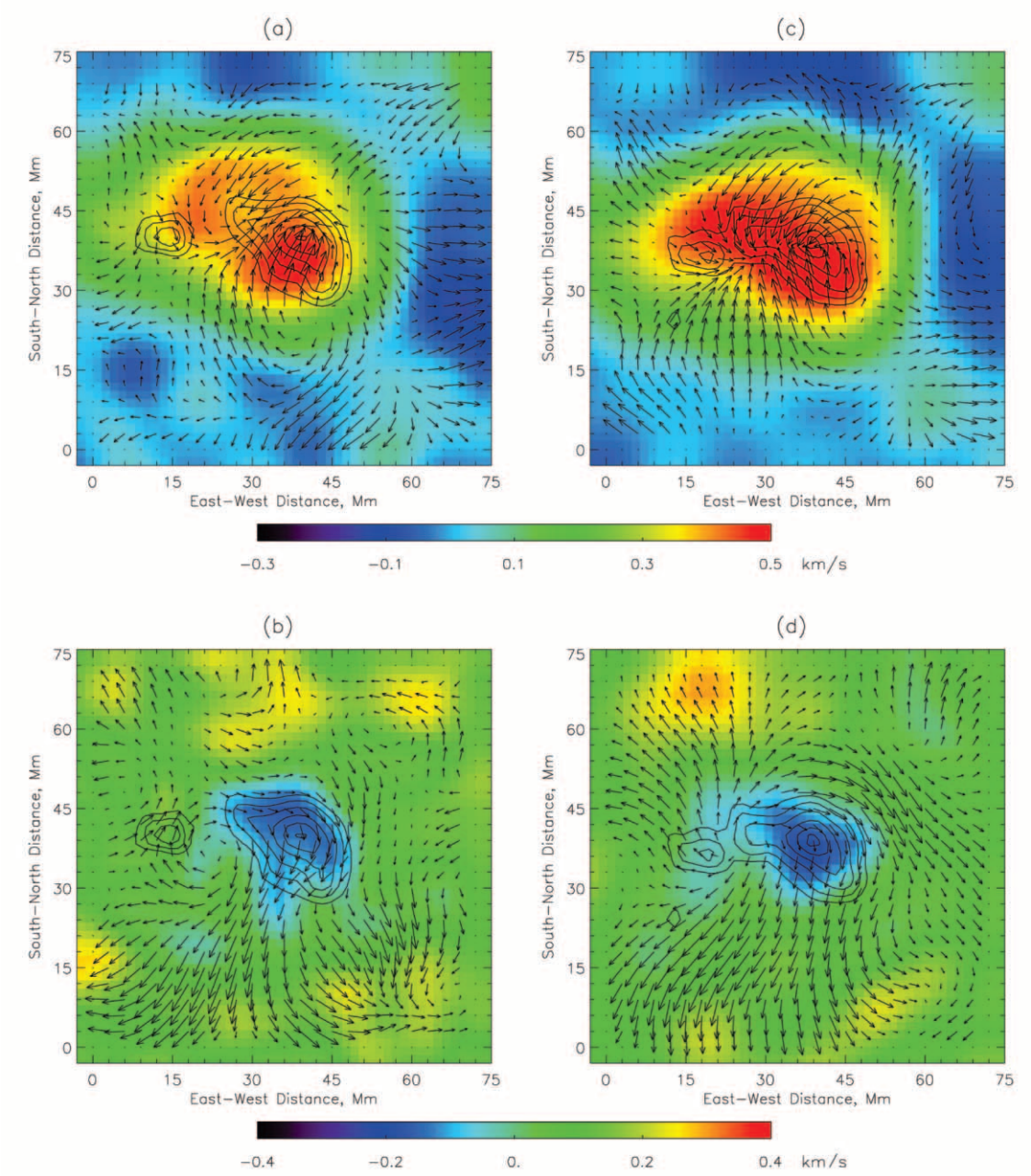

FIG. 4.—*Left*, Background image showing the vertical velocities and the horizontal velocity field (*arrows*) obtained from the August 7 data at depth intervals 0–3 (*top*) and 9–12 Mm (*bottom*); *right*, results for the August 8 data with the same depth intervals 0–3 (*top*) and 9–12 Mm (*bottom*). The longest arrow is 0.5 km s^{-1} for both the upper and lower graphs. The contour lines represent the line-of-sight magnetic field, the same as in Fig. 3.

(Mestel 1999). In particular, we use a component of α^v corresponding to the vertical components of velocity and vorticity: $\alpha_z^v = v_z(\partial v_y/\partial x - \partial v_x/\partial y)/(v_x^2 + v_y^2 + v_z^2)$. This corresponds to the current helicity obtained from magnetograms by some previous authors, e.g., Pevtsov, Canfield, & Metcalf (1995). After computing the value α_z at each pixel, we average these values over the whole active region where $B_z > 100$ G, although the selection of the 100 G threshold is arbitrary. The mean kinetic helicity from the August 7 velocity data (Figs. 4*a* and 4*b*) is -1.01×10^{-8} m^{-1} for the depth of 0–3 Mm, and -2.21×10^{-8} m^{-1} for the depth of 9–12 Mm, and the mean kinetic helicities for the August 8 data (Figs. 4*c* and 4*d*) are -2.11×10^{-8} and -6.26×10^{-8} m^{-1}, respectively.

Based on the observations of vector magnetograms in solar active regions, Pevtsov et al. (1995) calculated the mean current helicity of many active regions with the definition of current helicity as $\alpha = J_z/B_z$, where J_z is the line-of-sight current density and B_z is the line-of-sight magnetic field. The average kinetic helicity calculated from our inversion results of this active region has the same order of magnitude as the typical current helicity of active regions calculated by them. It is suggested by many authors (e.g., Longcope, Fisher, & Pevtsov 1998) that the magnetic helicity observed in the photosphere may be produced by helical motions beneath the photosphere. However, we can hardly draw any conclusion about the relationship between the subsurface kinetic helicity and the magnetic helicity from

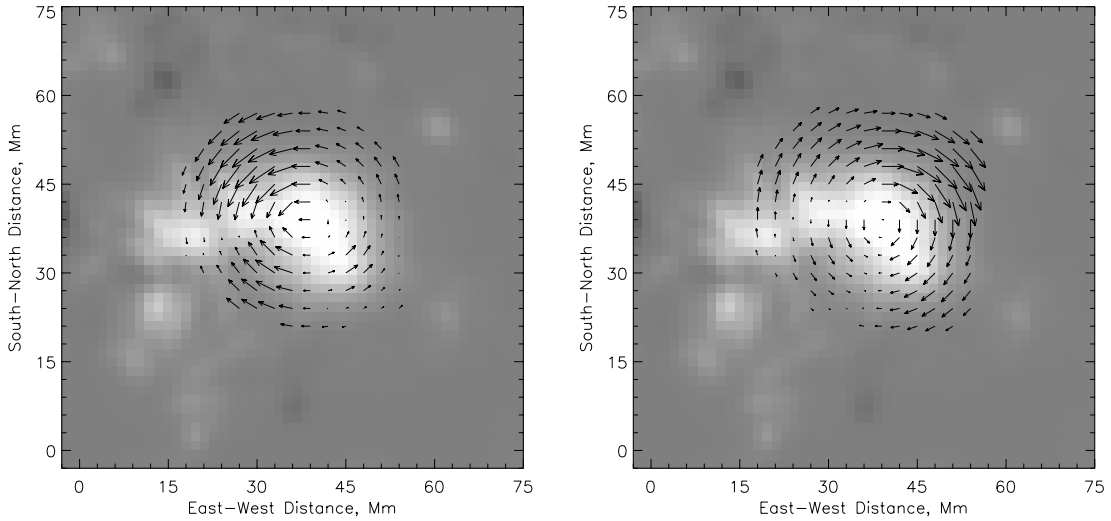

FIG. 5.—Tangential components of flow velocity relative to the center of the sunspot at two different depths, 0–3 (*left*) and 9–12 Mm (*right*), obtained from the August 8 data. The background images show the magnetic field the same as the contour in Fig. 3. The longest arrow in both graphs represents a speed of 0.45 km s^{-1}.

just the one sample that we currently have. Apparently, a statistical study combining the kinetic helicity and magnetic helicity is needed for better understanding this relationship in solar active regions.

4. ERROR ANALYSIS

4.1. *Monte Carlo Simulation*

The inverse problem of the time-distance helioseismology is reduced to the linear system $\mathbf{Ax} = \mathbf{b}$, which is solved by the method of least squares. The covariance matrix for error estimations of the inversion results is given by $C_m = \sigma_d^2 (\mathbf{A}^T\mathbf{A})^{-1}$ (see Menke 1984), where σ_d^2 is the covariance matrix from the observation data. However, it is not realistic to perform such a calculation because $(\mathbf{A}^T\mathbf{A})^{-1}$ is too large to calculate directly, and the LSQR algorithm does not give the matrix inverse explicitly, nor does the other algorithm, MCD. Therefore, we estimate the error propagation by Monte Carlo simulation.

Time-distance helioseismology calculates the wave propagation time by fitting the cross-covariance of the solar oscillation signals in two locations; hence, a fitting error of the propagation time can be estimated at each pixel for different travel distances by following the prescription in Press et al. (1992). Typically, the fitting errors are less than 2% of the wave propagation time. However, only the travel time differences are used for the inversion, which are relatively small and therefore have significant error levels. For larger distances, we use larger annulus intervals in which more data points are included, and in this case fitting errors are usually smaller than those from smaller distances. This is done to increase the reliability of the inferences for deeper layers. Then, for each specific distance, we approximate the fitting error distribution by a Gaussian function. Although the exact distribution function for the travel time–fitting errors is not exactly known, to the observed distributions the Gaussian function is a good approximation.

After the distribution function of the fitting errors is obtained for each distance, we perform Monte Carlo simulation by producing 40 sets of random errors consistent with the error distribution function and adding these to the travel time estimates for August 8 data. The time-distance inversion for three-dimensional velocity is performed for each of these 40 data sets, respectively. After the inversion is done, the mean value and standard deviation are computed for each pixel of the velocity maps. In Figure 6, the average of the mean values of the horizontal and vertical components of velocity are presented, and the error bars indicate the average of standard errors at different depths. We find that the results for the horizontal component of velocity are robust, while those for the vertical component of the velocity are more uncertain (we even have difficulty in determining the correct signs at the depth from 3 to 6 Mm). However, in the depth intervals 0–3 and 9–12 Mm, which are used in our analysis of the vortical flows (shown in Fig. 4), the errors are relatively small.

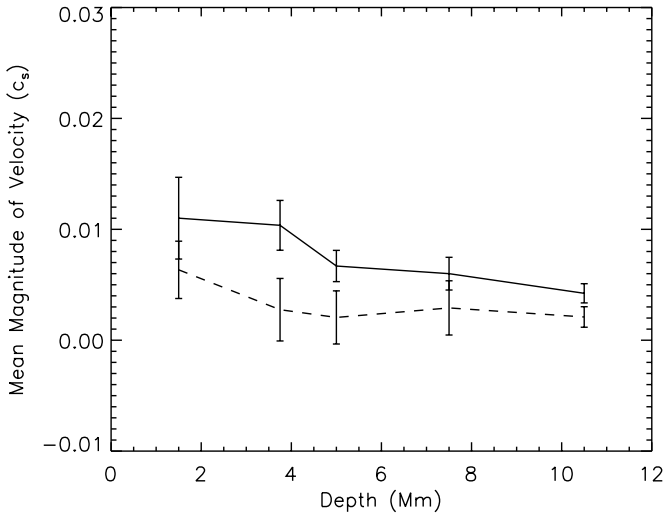

FIG. 6.—Mean magnitude of the horizontal (*solid line*) and vertical (*dashed line*) components of flow velocity at different depths with the error bars estimated by a Monte Carlo simulation. The velocities are shown in the unit of local sound speed.

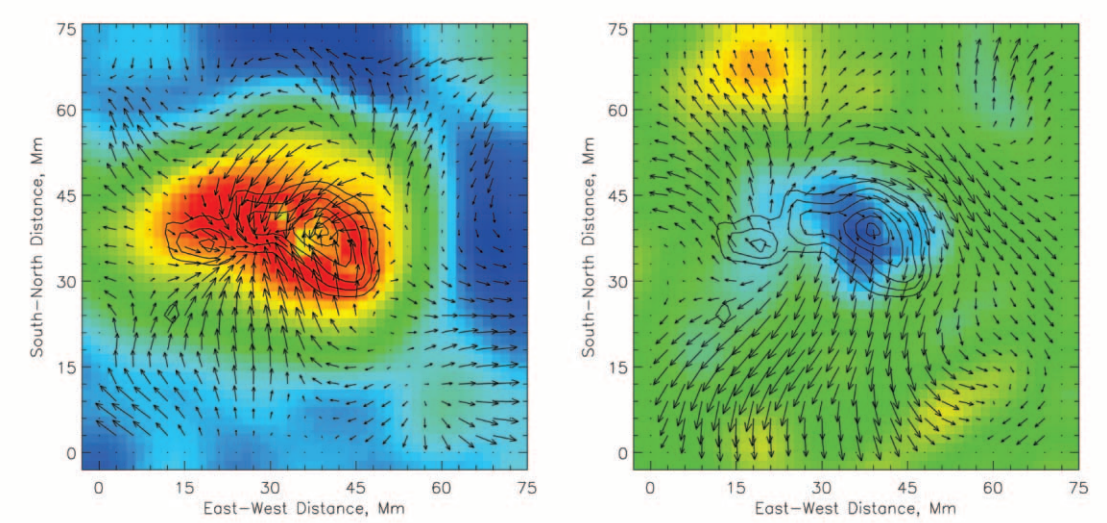

FIG. 7.—Flow fields derived for the August 8 data after masking the sunspot umbra (see text). Color index and arrows are the same as in Fig. 4.

4.2. *Umbra Mask Test*

The other issue that we need to consider is the *SOHO*/MDI observation saturation problem in dark areas of sunspots umbrae,[1] which appears in MDI magnetograms and Dopplergrams observations when the spectral line intensity drops below a certain level. A possible additional effect on our measurements is a strong absorption of the solar acoustic power by sunspot umbrae (Braun, Duvall, & Labonte 1988).

To test how the saturation and the acoustic absorption in sunspot umbra might affect the vortical flow fields derived from our analysis, we discard all the travel times obtained inside the sunspot umbra and then perform the inversion calculations, although only a small part of the umbra is affected by the saturation. The results are shown in Figure 7. We find from the masked data that at the depth of 0–3 Mm the downward flow speeds are only slightly smaller than those in the original calculation, and the horizontal speeds also change slightly, but most importantly, the flow structure is not affected. We still see the same downward and converging flow patterns, thus confirming the earlier conclusion of Zhao et al. (2001). Outside the sunspot umbra, the vortical flows seen in Figure 4 remain almost the same. At the depth of 9–12 Mm, the flow fields are not affected at all by the umbral mask. Therefore, we conclude that the potential uncertainties in the observations of the umbra area do not significantly affect our results.

5. DISCUSSION

Using the time-distance technique and inversion methods based on the ray approximation, we have mapped the sound speed variation structures and flow fields beneath a rotating sunspot. We have estimated the error propagation in both the time-distance measurements and the inversion procedure by Monte Carlo simulations and found that, while the velocity inferences may have significant errors, estimates of the horizontal component are sufficiently robust for determining the structure of the vortical flows. The test of masking the sunspot umbra where the measurements may be uncertain because of the observational signal saturation and wave absorption showed only slight changes in both components of the velocity in the sunspot area close to the surface and nearly no change in the deeper layers. Perhaps the main uncertainty of our measurements comes from the ray approximation in the inversion procedure, which is known to underestimate the magnitude of perturbations, particularly on small scales (Birch et al. 2001). However, the larger scale structure of sunspots should be reproduced correctly (Jensen et al. 2001). Hence, results shown in this paper are correct qualitatively, if not quantitatively.

Many previous observations have revealed that the magnetic field in some active regions is twisted. Evidence for the twists is exhibited in various solar phenomena, such as the morphology of Hα structures (Hale 1927), filaments (Martin, Billamoria, & Tracadas 1994), and coronal loops (Rust & Kumar 1996). The results presented in Figure 3 show us that the surface magnetic field of a rapidly rotating sunspot has a twisted angle with respect to the subsurface sound speed structure at the depth of 6 Mm. This provides observational evidence that magnetic flux twists also exist beneath the visible surface of the active region, in addition to the previously reported twists in the solar photosphere and corona. Furthermore, it was argued by Leka, Canfield, & McClymont (1996) and many other investigators that the magnetic field twists may have already formed before the emergence of magnetic flux on the surface. Our observation presents direct evidence that magnetic field twists may exist beneath the surface.

Assuming that the magnetic flux tubes have already been twisted below the solar surface, Magara & Longcope (2003) simulated numerically the emergence process of magnetic flux and reproduced the sigmoidal shape of coronal loops as observed in X-rays. In addition, the vortical flows in and around the magnetic flux footpoints were also found in their simulations, which in turn could further twist the already twisted magnetic flux. Our observation of the sunspot rotation in the photosphere and 5 Mm below the photosphere seems to be consistent with their numerical simulation for both the subsurface magnetic twists and the photospheric

[1] See http://soi.stanford.edu/general/TechNotes/01.144/TN01-144.pdf.

and subphotospheric vortical motions. Perhaps our inference of the subsurface vortical flow fields in this study may also support the argument by López Fuentes et al. (2003) that vortical flows may exist in subphotosphere and play important role in the formation of magnetic twists.

It is widely believed that vortical sheared flows around magnetic flux footpoints could eventually lead to solar eruptions. Recently, some authors began to calculate the energy and magnetic helicity generated by the surface flows. Some argued that the surface horizontal rotational flows could provide sufficient magnetic helicity and energy to produce solar flares (Moon et al. 2002), while others argued that magnetic helicity from subsurface must be included to be sufficient for solar eruptions (Nidos & Zhang 2002). Our observation shows that strong subsurface vortical flows should be taken into account as a potential source of magnetic helicity and energy buildup, which can be much stronger in the deeper layers than at the surface because mass density and plasma β are much higher there.

In this study, we have found counterclockwise vortical flows at the depth range of 0–3 Mm around the sunspot (which also rotated counterclockwise at the surface), and the evidence of counterclockwise flows at the depth of 9–12 Mm. What could cause these opposite vortical flows is an open question. At present there is no theoretical model explaining the vortex motions. It may be useful to consider some analogies. For instance, it is known that for hurricanes on the Earth there are strong converging flows near the ocean surface and divergent flows up in the high altitude of the atmosphere; hence, the hurricanes have counterclockwise flows at the bottom and clockwise flows at the top due to the Coriolis force on the Earth's Northern Hemisphere (see Gordon 1998). If one can think of a sunspot model as a reverse hurricane as proposed by Schatten & Mayr (1985), then the opposite vortical flows may be caused by Coriolis force. If this were the case, then magnetic flux can be twisted by these flows and hence build up a great amount of energy. However, if the reverse-hurricane sunspot model is true, the question is why the vortical flows are not observed in most sunspots.

By using the time-distance inferences, we have also calculated the subsurface kinetic helicity in two different depth intervals and obtained the kinetic helicity values of the same order of magnitude as the current helicity of typical active regions. It is reasonable to believe that kinetic helicity and magnetic helicity are related to each other in the subphotosphere and upper convection zones, and the subsurface kinetic helicity may make some contribution to the formation of surface magnetic helicity and its hemispherical preference distribution. Certainly, how the subsurface kinetic helicity is correlated with the surface magnetic helicity needs a further statistical study. The time-distance inversion technique and results presented in this paper enable us to carry out such a study.

Further time-distance helioseismology studies of the subsurface dynamics of sunspots and active regions, particularly before powerful solar flares, may be of great importance for the investigation of the subsurface energy buildup, kinetic helicity development, and their relationship to solar eruptive events and may make forecasting solar eruptions possible.

The *SOHO*/MDI project is supported by NASA grant NAG 5-3077 to Stanford University. *SOHO* is a project of international cooperation between ESA and NASA.

REFERENCES

Birch, A. C., & Kosovichev, A. G. 2000, Sol. Phys., 192, 193
Birch, A. C., Kosovichev, A. G., Price, G. H., & Schlottmann, R. B. 2001, ApJ, 561, L229
Braun, D. C., Duvall, T. L., Jr., & Labonte, B. J. 1988, ApJ, 335, 1015
Braun, D. C., & Lindsey, C. 2000, Sol. Phys., 192, 285
Brown, D. S., Nightingale, R. W., Alexander, D., Schrijver, C. J., Metcalf, T. R., Shine, R. A., Title, A. M., & Wolfson, C. J. 2003, Sol. Phys., submitted
Canfield, R. C., & Pevtsov, A. A. 2000, J. Astrophys. Astron., 21, 213
Chou, D.-Y. 2000, Sol. Phys., 192, 241
Duvall, T. L., Jr., D'Silva, S., Jefferies, S. M., Harvey, J. W., & Schou, J. 1996, Nature, 379, 235
Duvall, T. L., Jr., Jefferies, S. M., Harvey, J. W., & Pomerantz, M. A. 1993, Nature, 362, 430
Giles, P. M. 1999, Ph.D. thesis, Stanford Univ.
Gizon, L., & Birch, A. C. 2002, ApJ, 571, 966
Gordon, A. H. 1998, Dynamic Meteorology: A Basic Course (Oxford: Oxford Univ. Press)
Haber, D. A., Hindman, B. W., Toomre, J., Bogart, R. S., Thompson, M. J., & Hill, F. 2000, Sol. Phys., 192, 335
Hale, G. E. 1927, Nature, 119, 708
Jacobsen, B. H., Møller, I., Jensen, J. M., & Effersø, F. 1999, Phys. Chem. Earth, 24, 15
Jensen, J. M., Duvall, T. L., Jr., Jacobsen, B. H., & Christensen-Dalsgaard, J. 2001, ApJ, 553, L193
Jensen, J. M., Jacobsen, B. H., & Christensen-Dalsgaard, J. 2000, Sol. Phys., 192, 231
Knoška, S. 1975, Bull. Astron. Inst. Czechoslovakia, 26, 151
Kosovichev, A. G. 1996, ApJ, 461, L55
———. 1999, J. Comput. Appl. Math., 109, 1
Kosovichev, A. G., Duvall, T. L., Jr., & Scherrer, P. H. 2000, Sol. Phys., 192, 159
Leka, K. D., Canfield, R. C., & McClymont, A. N. 1996, ApJ, 462, 547
Lindsey, C., & Braun, D. C. 2000, Sol. Phys., 192, 261
Longcope, D. W., Fisher, G. H., & Pevtsov, A. A. 1998, ApJ, 507, 417
López Fuentes, M. C., Démoulin, P., Mandrini, C. H., Pevtsov, A. A., & van Driel-Gesztelyi, L. 2003, A&A, 397, 305
Magara, T., & Longcope, D. W. 2003, ApJ, 586, 630
Martin, S. F., Billamoria, R., & Tracadas, P. W. 1994, in Solar Surface Magnetism, ed. R. J. Rutten & C. J. Schrijver (Dordrecht: Kluwer), 303
Menke, W. 1984, Geophysical Data Analysis: Discrete Inverse Theory (New York: Academic Press)
Mestel, L. 1999, Stellar Magnetism (Oxford: Oxford Univ. Press), 195
Moon, Y.-J., Chae, J., Choe, G. S., Wang, H., Park, Y. D., Yun, H. S., Yurchyshyn, V., & Goode, P. R. 2002, ApJ, 574, 1066
Nidos, A., & Zhang, H. 2002, ApJ, 573, L133
Paige, C. C., & Saunders, M. A. 1982, ACM Trans. Math. Software, 8, 43
Pevtsov, A. A., Canfield, R. C., & Metcalf, T. R. 1995, ApJ, 440, L109
Press, W. H., Teukolsky, S. A., Vetterling, W. T., & Flannery, B. P. 1992, Numerical Recipes in FORTRAN 77 (2d ed.; Cambridge: Cambridge Univ. Press), 675
Rust, D. M., & Kumar, A. 1996, ApJ, 464, L199
Schatten, K. H., & Mayr, H. G. 1985, ApJ, 299, 1051
Scherrer, P. H., et al. 1995, Sol. Phys., 162, 129
Sun, M. T., et al. (TON Team). 2002, Sol. Phys., 209, 5
Tokman, M., & Bellan, P. M. 2002, ApJ, 567, 1202
Zhao, J., & Kosovichev, A. G. 2003, in Proc. *SOHO* 12/GONG+ 2002 Workshop, Local and Global Helioseismology: The Present and Future, ed. H. Sawaya-Lacoste (ESA SP-517; Noordwijk: ESA), 417
Zhao, J., Kosovichev, A. G., & Duvall, T. L., Jr. 2001, ApJ, 557, 384